Analysis of Electromagnetic Transient and Adaptability of Second-Harmonic Restraint Based Differential Protection of UHV Power Transformer

Xiangning Lin, *Senior Member, IEEE*, Jingguang Huang, Linjun Zeng, and Zhiqian Q. Bo, *Senior Member, IEEE*

***Abstract*—An autotransformer is used as the main type of UHV transformer, but the internal fault model of autotransformer provided by most simulation software is not available. To find out the existing problems of the application of the differential protection of UHV transformer, a three winding autotransformer model is firstly built according to the existing Unified Magnetic Equivalent Circuit transformer model provided by EMTDC software. Furthermore, the internal fault model of UHV transformer is set up. By virtue of above models, the energization and internal faults are simulated to validate the well-applied differential protection using second-harmonic blocking. It can be proven that the second-harmonic ratios of three phase inrushes of the UHV power transformer are all below 10% in some energization scenarios. In this case, the maloperation of the differential protection by means of 15% $\sim$ 20% second-harmonic restraint ratio cannot be avoided. On the other hand, the second-harmonic ratio of the fault current is relatively high in the beginning of fault inception for some light faults, leading to the short time delay of operation of protection. This discovery will encourage the research and development of the novel scheme of the main protection of UHV transformer.**

***Index Terms*—Autotransformer, EMTDC, harmonic, inrush, internal fault, UHV.**

I. Introduction

THERE has been a problem of distinguishing between the magnetic inrush and the fault current for the differential protection of the power transformer [1]–[4], and this challenge that the protection of 1000 kV ultra high voltage (UHV) transformer faces is possibly more serious. Compared with extra high voltage (EHV) power systems, the electromagnetic environment of UHV systems is more complex. Meanwhile, the configuration and parameters of UHV transformer differ from EHV transformer obviously. In this case, the preconditions of applying transformer differential protection correctly rest with the modeling of UHV power transformer reasonably and appropriate analysis of corresponding electromagnetic transient.

An utotransformer is the main type of UHV transformer. However, the model of the autotransformer is not available in most simulation software. An ordinary countermeasure is to replace the autotransformer by the common transformer when executing electromagnetic transient simulations [5]. In this case, the effect of magnetic coupling can be included, but the electric relation between primary side and secondary side cannot be involved. The model proposed in [6] adopts the flux linkage as the state variable and includes the nonlinearity of transformer core. It is clear in terms of concept but too complex to perform in many cases. In [7], a new transient simulation model of the three-phase autotransformer is described, in which the controlled voltage and current sources are developed with the modified damping trapezoidal method which is engaged to form the synthetic simulation model. In this case, both the efficiency and the precision of simulations are improved. However, this type of model will be more reasonable if it takes into account the nonlinearity of magnetizing impedance. Furthermore, the electromagnetic transient simulations in the UHV electromagnetic environment are new challenges, especially when including the UHV transmission line with distributed parameters.

PSCAD/EMTDC is typical simulation software applied in various fields of power systems. In particular, it is suitable for electromagnetic transient simulations. In this paper, according to the equivalent circuit of three-winding autotransformer, we set up the UHV autotransformer model and its internal faults model by means of a unified magnetic equivalent c ircuit (UMEC) transformer model provided by EMTDC software. This new model takes into accounted both the particularity of UHV transformer and the nonlinearity of the transformer core. Based on this model, we carried out a variety of simulations tests, including energization, inter-turn short-circuited faults, phase-to-ground short-circuited faults and phase-to-phase short-circuited faults. Finally, we analyzed the current waveforms and evaluated the issues of the transformer differential protection using second-harmonic blocking scheme applied in UHV transformer protections.

II. Modeling of the UHV Power Transformer

A. Basic Configuration of the UHV Power Transformer

Autotransformer is applied widely in 220 kV and higher systems due to many merits such as low cost, high efficiency,

Manuscript received December 17, 2009; revised April 07, 2010. Date of publication June 14, 2010; date of current version September 22, 2010. This work was supported in part by the National Natural Science Foundation of China (50777024), and in part by the Program for New Century Excellent Talents in University (NCET-07-0325), by the National High Technology Research and Development Program of China (2008AA05Z214), by the Major State Basic Research Development Program (2009CB219700), and in part by the State Grid Company Key Programs (under Grant SGKJJSKF (2008) 469 and the one approved in 2009). Paper no. TPWRD-00936-2009.

X. Lin and J. Huang Han are with Electric Power Security and High Efficiency Lab, Huazhong University of Science and Technology (HUST), Wuhan 430074, China and the College of Electrical Engineering and Information Technology, Three Gorges University, Yichang 443002, Hubei Province, China (e-mail: linxiangning@hotmail.com).

L. Zeng is with the College of Electrical Engineering and Information Technology, Three Gorges University, Yichang 443002, Hubei Province, China.

Z. Q. Bo is with AREVA T&D-Automation & Information Systems, Stafford ST17 4LX, U.K.

Color versions of one or more of the figures in this paper are available online at http://ieeexplore.ieee.org.

Digital Object Identifier 10.1109/TPWRD.2010.2050343

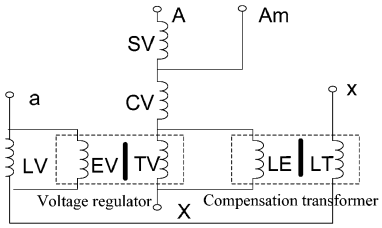

Fig. 1. Principle diagram of UHV transformer voltage regulation.

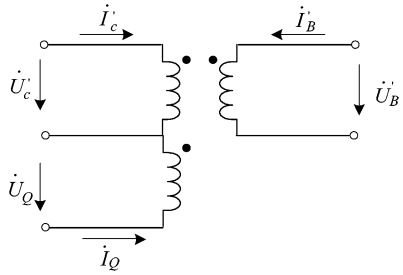

Fig. 2. Three-winding auto transformer theory diagram.

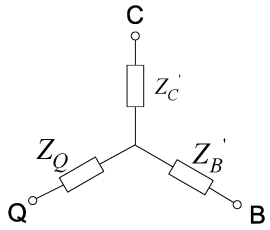

Fig. 3. Three ports Y-type equivalent circuit.

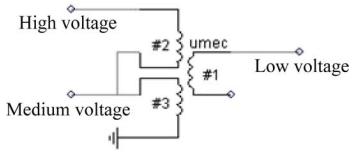

Fig. 4. Model of the UHV transformer.

low exciting power and so on. The tremendous capability and the high requirement of insulation lead to the huge bulk and prodigious weight of UHV transformers as the single-phase capability of UHV transformer is up to 1000 MVA. In view of the convenience of transportation, single-phase configuration is necessary. The UHV transformer produced in China is exactly the single-phase autotransformer [8]. The three-phase configuration is implemented with the single-phase transformer bank.

Autotransformer has a tertiary winding, namely the low-voltage winding. The tertiary winding is unloaded. Instead, its functionality rests with the circulation of the third harmonic. Three phases of the tertiary winding are connected by delta-type and earthed through a low-voltage reactor.

To meet the demand of electric isolation, the nonexciting voltage-regulating from the neutral terminal is adopted and the voltage regulator and compensation transformer separately are set by the UHV transformer. The principle can be illustrated by Fig. 1.

SV, CV, LV, TV, EV, LE, and LT, respectively, represent series winding, common winding, low-voltage winding, voltage regulation winding, magnetizing winding, low-voltage magnetizing winding, and low-voltage compensation winding. Due to this special type of coupling of windings, the short-circuited impedance of the UHV transformer is much bigger than that of the ordinary transformer.

Since the currents of all sides of the UHV transformer are the main concerns, the main transformer and the corresponding voltage-regulating compensation transformer are equivalent to being a three-winding autotransformer.

B. The Equivalent Circuit of Three-Winding Autotransformer

No mater how the windings are arranged, the three-winding autotransformer can be studied by means of a equivalent Y-type equivalent circuit [9]. In the following, the equivalent circuit of the UHV transformer based on the series, common and tertiary winding are modeled.

As seen in Fig. 2, converting electrical quantities to common winding side, $\dot{U}_c'$ and $\dot{I}_c'$ are the voltage and the current, respectively, of the series winding. The voltage and the current of the common winding are denoted by $\dot{U}_Q$ and $\dot{I}_Q$. Besides, $\dot{U}_B'$ and $\dot{I}_B'$ represent the voltage and the current of the tertiary winding.

Similar to the ordinary three-winding transformer, the following equation can be deduced when the exciting current is ignored, as given by:

$$\begin{cases} \dot{U}_C' - \dot{U}_Q = \dot{I}_C' Z_C' + \dot{I}_Q Z_Q \\ \dot{U}_C' - \dot{U}_B' = \dot{I}_C' Z_C' + \dot{I}_B' Z_B' \end{cases} \quad (1)$$

where Z_C' is the leakage impedance converted from the series winding, Z_Q is the leakage impedance of the common winding, and Z_B' is the leakage impedance converted from the low-voltage winding.

According to (1), its Y-type equivalent circuit can be deduced as seen in Fig. 3.

The parameters of the equivalent circuit can be obtained from the tests of the ordinary three-winding transformer. By this arrangement, the three-winding autotransformer can be simulated based on the ordinary three-winding transformer.

C. Models of UHV Transformer for Simulation

In this paper, modeling of UHV transformer and simulation of electromagnetic transient are both carried out by virtue of EMTDC. However, EMTDC does not provide the three-winding autotransformer models directly. According to the above analysis, and in view of the "electric" relation between the series winding and the common winding of autotransformer, we connect two windings of the UMEC three-winding transformer model to form the high-voltage winding and the medium-voltage winding. In this way, UHV transformer model can be obtained.

As seen in Fig. 4, #1 winding, #2 winding, and #3 winding denote the low-voltage winding, the series winding and the common winding respectively. The validation of the equivalence is to guarantee the leakage impedances of corresponding windings being equal between the equivalent model and the original model. Significantly, the parameters of the UHV transformer should be converted to the side of the tertiary winding.

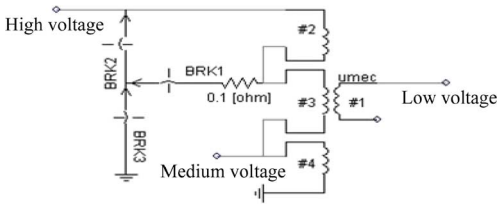

Fig. 5. Internal faults model of transformer.

The UMEC transformer model is built primarily based on the core geometry. Unlike the classical transformer model, the magnetic coupling between windings of different phases is taken into account in the UMEC model in addition to coupling between windings of the same phase. The piecewise technique is used to control the conductance of equivalent branch. The nonlinearity characteristic of the core is input directly into the model as a piece-wise U-I curve, which makes full use of the interpolation algorithm for the calculation of exact instants when the state changes.

Internal faults of the transformer include inter-turn short-circuited faults, turn-to-ground faults, lead-out phase-to-phase short-circuited faults and lead-out phase-to-ground faults. The modeling of internal winding faults is the main concern of this paper.

When an inter-turn fault occurs on the dual-winding transformer, the faulty turns of the faulty winding can be regarded as a tertiary winding [10]. Based on this concept, the faulty turns of the three-winding transformer can be simulated by a fourth winding, see Fig. 5.

In Fig. 5, #2 winding denotes the faulty turns, and the fault types can be controlled by the breakers. The leakage reactance X_2 of #2 winding and the leakage reactance X_3 of 3# winding can be calculated, as given by

$$\begin{cases} X_2 + X_3 = X_c \\ X_2/X_3 = (N_2/N_3)^2 \end{cases}. \tag{2}$$

In (2), X_c is known as the leakage reactance of the series winding. N_2 and N_3 are, respectively, the turn quantities of #2 winding and #3 winding. Practically, N_2/N_3 nearly is equal to the ratio of #2 winding's rated voltage to #3's windings.

Based on Fig. 5, the interturn fault with short-circuit turn ratio lower than 50% and the turn-to-ground fault with short-circuit turn ratio bigger than 50% can be simulated. To simulate the else ones, we can change the position of #4 winding with #2 and #3 winding and keep the places of breaker unchanged. In this case, one end of #4 winding is connected to the terminal of HV side and the other one is connected to one end of #2 winding. By virtue of this arrangement, we can investigate the internal faults of UHV transformer thoroughly.

D. Verification of the Proposed Autotransformer Modeling Method

The feasibility of the model proposed in part C can be testified by means of the following way. Actually, the benchmark model of two-winding autotransformer is available in the EMTDC package. Meanwhile, the conventional two-winding transformer is available as well. Then, we can follow the auto-

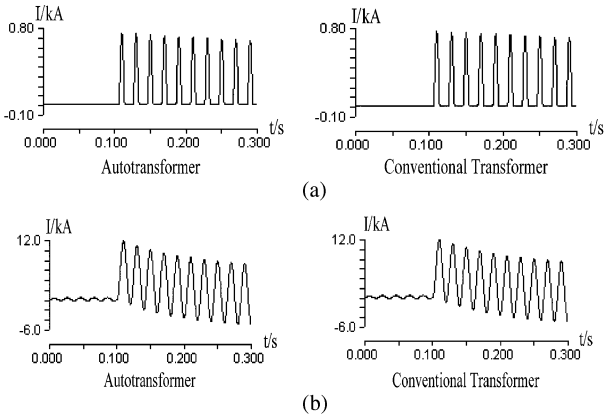

Fig. 6. Comparison of two models. (a) Energization from HV side. (b) Lead-out fault on LV side.

transformer modeling method proposed in part C to connect the windings of two conventional transformers by connecting one terminal of one winding to that of the other one. Therefore, the autotransformer can be established. Based on this model, the energization and faults are simulated. Meanwhile, the benchmark model of the two-winding autotransformer in EMTDC is equipped with the same parameters and applied with the same disturbances. By virtue of the comparison of the simulated current waveforms, the proposed method can be verified.

The parameters of a two-winding autotransformer are set as follows: capacity: 100 MVA, rated voltage: 460 kV/230 kV, leakage impedance: 5% (with respect to the base of HV side), no-load loss: 80 kW, short-circuit loss: 150 kW. According to the criterion of guarantee the identical leakage impedance, the parameters of the conventional transformer used to simulate the above autotransformer are set as follows by the appropriate converting computation: capacity: 100 MVA, rated voltage: 230 kV/230 kV, leakage impedance: 20% (with respect to the base of the primary side), no-load loss: 80 kW, short-circuit loss: 640 kW. A variety of scenarios are simulated in the same environment. Two typical scenarios can refer to Fig. 6. Among which, Fig. 6(a) shows the comparison of the energization, and Fig. 6(b) shows the comparison of the lead-out faults.

As seen, the current waveforms resulting from the same simulation case are identical. Therefore, the proposed modeling method is verified.

III. Simulation and Analysis

Due to the nonlinearity of the transformer core, the magnetizing inrush possibly occurs when a transformer is energized, which easily leads to the maloperation of the differential protection if no blocking strategy is included. Therefore, the identification of the inrush current is the premise of the correct operation of the differential protection. In the following, the above two models are used to simulate the energization and internal faults of UHV transformer. In this way, the operation behavior of the protection can be investigated rationally.

A. System Model and Correlative Parameters

The system model comes from Jindongnan-Nanyang-Jingmen 1000 kV AC test and demonstration project of

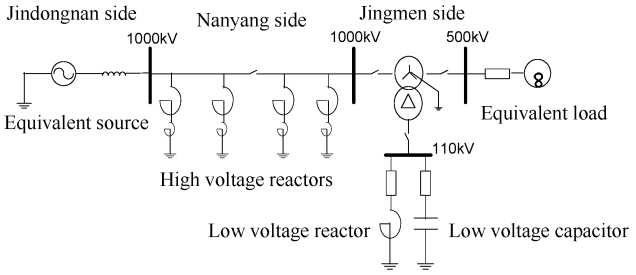

Fig. 7. System model.

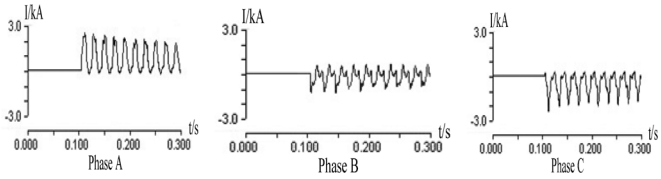

Fig. 8. Magnetic inrush currents in the condition of typical energization, Initial angle of phase A is 0°; remnant flux densities of the three phase are all 0.

TABLE I
HARMONIC ANALYSIS OF INRUSH CURRENTS

Remnant flux density	Initial angle of phase A (°)	2nd harmonic ratio (%)		
		Phase A	Phase B	Phase C
Phase A:0B_m Phase B:0B_m Phase C:0B_m	0	30.4	40.4	15.1
	30	31.8	22.6	14.8
	60	37.0	23.7	34.3
Phase A:0.7B_m Phase B:-0.5B_m Phase C:-0.5B_m	0	16.0	18.9	10.1
	30	17.0	15.4	1.9
	60	30.3	15.0	3.7
Phase A:0.9B_m Phase B:0B_m Phase C:-0.9B_m	0	12.8	17.7	4.0
	30	9.8	6.9	6.1
	60	17.0	17.0	7.8

CHINA, and all the parameters in the model system are from the real UHV project.

The transmission line parameters are given as follows:

Jindongnan-Nanyang: $\text{length} = 363\ \text{km}$; Positive sequence resistance in per km $\text{R}_1 = 0.00758\ \Omega/\text{km}$, positive sequence reactance in per km $\text{X}_1 = 0.26365\ \Omega/\text{km}$, positive sequence capacitance in per km $\text{C}_1 = 0.01397\ \mu\text{F/km}$. Zero sequence resistance $\text{R}_0 = 0.15421\ \Omega/\text{km}$, zero sequence reactance $\text{X}_0 = 0.7821\ \Omega/\text{km}$, zero sequence capacitance $\text{C}_0 = 0.008955\ \mu\text{F/km}$. Nanyang-Jingmen: $\text{length} = 291\ \text{km}$. Positive sequence resistance in per km $\text{R}_1 = 0.00801\ \Omega/\text{km}$, positive sequence reactance in per km $\text{X}_1 = 0.2631\ \Omega/\text{km}$, positive sequence capacitance in per km $\text{C}_1 = 0.013830\ \mu\text{F/km}$. Zero sequence resistance $\text{R}_0 = 0.1563\ \Omega/\text{km}$, zero sequence reactance $\text{X}_0 = 0.8306\ \Omega/\text{km}$, zero sequence capacitance $\text{C}_0 = 0.009296\ \mu\text{F/km}$.

The parameters of the UHV autotransformer are as follows: Rated capabilities of the high-voltage side, the medium-voltage side and the low-voltage side are, respectively, 1000 MVA, 1000 MVA, and 334 MVA. The voltage ratings of the high-voltage side, the medium-voltage side and the low-voltage side are, respectively, 1050 kV, 525 kV, and 110 kV.

The parameters of the short-circuited impedances (based on rated capabilities of the high voltage side) are as follows:

The short-circuited impedance is 18% in high-medium side, 62% in high-low side, and 40% in medium-low side.

No-load loss is 0.07%, magnetizing loss is 155 kW.

The rated capability of the high voltage reactors are given as below:

The rated capability is 960 MVA in Jindongnan side of Jindongnan-Nanyang transmission line, while 720 MVA in Nanyang side. The rated capability is 720 MVA in Nanyang side of Nanyang-Jingmen transmission line, and 600 MVA in Jingmen side.

In view of the influences which result from the energization transient of the transmission lines and high voltage reactors, the energization position is at the high voltage side of UHV transformer at Jingmen side.

The configuration of the system model is shown in Fig. 7.

As seen, the UHV source is connected to the high-voltage side of the UHV transformer via UHV transmission lines. The medium-voltage side is linked with an equivalent load, while low-voltage winding is connected in delta-type and is grounded through a reactor and a capacitor for compensation.

Actually, the source of the UHV project is provided by the medium-voltage side of the UHV transformer at Jindongnan. It is no harm to replace Jindongnan by an equivalent source since the emphasis rests with the energization at Jingmen. Besides, the reactors are modeled by the parallel inductances, and capacitors are modeled by capacitances. The remnant flux is modeled by the dc source which is put on the high-voltage side of the UHV transformer.

B. Simulation and Analysis of Energization

Energization simulations are carried out in terms of diverse initial angles and remnant fluxes. A scenario of typical inrush waveforms of three phases is shown in Fig. 8. As seen, the harmonics of the inrush is more abundant than the transformer's in EHV and lower level systems, leading to the more abnormal waveforms.

The UHV transformer adopts Y-d-11 type. Therefore, our concern focuses on the differential current, which determines whether the differential protection can operate correctly or not. The differential current is the summation of three-side influx currents. Therefore, the phase and magnitude compensation should be done instead of summation directly. Namely, if the influx currents of the high, medium, low voltage sides of phase A are $\dot{I}_{ah}$, $\dot{I}_{am}$ and $\dot{I}_{al}$, and the influx currents of the high, medium and low voltage side of phase B are $\dot{I}_{bh}$, $\dot{I}_{bm}$ and $\dot{I}_{bl}$, in view of the phase compensation and magnitude compensation, the differential current of phase A should be $(\dot{I}_{ah} - \dot{I}_{bh}) + ((525/\sqrt{3})/(1050/\sqrt{3}))(\dot{I}_{am} - \dot{I}_{bm}) + (110/(1050/\sqrt{3}))\dot{I}_{al}$. Because the transformer is energized at the high-voltage side, there are no currents in other two sides. Therefore, the differential current of phase A is $(\dot{I}_{ah} - \dot{I}_{bh})$ exactly. Table I shows the harmonic ratios of the three-phase differential currents in the condition of various energizations.

TABLE II
CONTENTS OF THIRD AND ABOVE HARMONICS WITH RESPECT TO THE SCENARIO IN TABLE I

Remnant flux density	Initial angle of phase A (o)	3rd harmonic ratio (%)	4th harmonic ratio (%)	5th harmonic ratio (%)	6th harmonic ratio (%)	7th harmonic ratio (%)
A:0B_m B:0B_m C:0B_m	0	31.1/46.3/25.4	6.3/18.6/12.8	6.4/13.1/2.5	4.7/3.8/4.3	4.9/7.0/4.7
	30	23.8/10.1/10.8	21.4/14.5/18.4	4.1/12.9/8.3	6.3/4.7/6.8	7.0/8.2/3.8
	60	32.3/23.3/29.5	21.3/14.1/12.2	9.1/2.6/3.2	5.9/5.6/3.1	10.0/7.8/4.0
A:0.7B_m B:-0.5B_m C:-0.5B_m	0	24.5/41.1/19.0	11.4/17.4/3.8	6.6/6.9/7.3	3.8/6.9/0.3	3.0/5.5/2.7
	30	30.5/23.7/9.5	14.7/8.0/14.2	8.6/9.7/1.1	4.2/7.6/4.5	7.0/6.3/6.0
	60	37.1/24.6/7.6	12.3/10.2/10.5	7.7/11.7/5.0	4.4/2.9/4.4	3.5/4.6/5.2
A:0.9B_m B:0B_m C:-0.9B_m	0	35.4/24.7/22.3	6.5/12.8/7.1	9.3/6.2/5.1	5.2/6.8/2.6	2.3/8.6/4.3
	30	27.7/33.4/10.2	12.0/15.1/16.6	7.9/6.7/2.5	7.8/5.9/6.9	5.4/8.5/8.5
	60	50.0/24.6/33.4	20.0/8.8/17.3	7.0/6.7/5.4	4.9/2.1/1.8	3.4/3.3/4.4

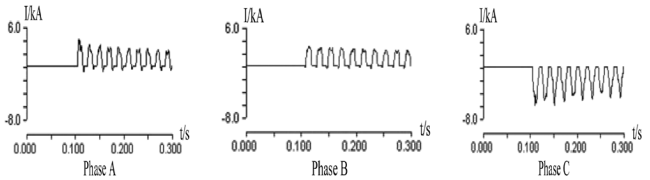

Fig. 9. Magnetic inrushes leading to the maloperation of different ial protection.

According to Table I, when the initial angle of phase A is 30°, the harmonic ratio of one phase will be under 15%, even if no remnant flux exists. If the remnant flux is taken into account, the harmonic ratio of phase C will fall below 1.9%, as shown in fifth row of Table I. This indicates that it is unrealistic to only adjust the harmonic restraint ratio to avoid the maloperation of the differential protection. Above maloperation cannot be avoided unless by virtue of adopting such a blocking strategy that the protection is blocked as the second-harmonic ratio of any one phase exceeds the threshold and regulating the harmonic restraint ratio to 15%. Furthermore, when the remnant fluxes of three phases are 0.9 Bm, 0 and −0.9 Bm, and the initial angle of phase A is 30°, the second-harmonic ratios of three phase differential currents are all under 10%, of which the corresponding waveforms are shown in Fig. 9. In this case, even the above strict countermeasure cannot allow the protection to survive.

In this scenario, the maloperation is also unavoidable even though above-mentioned blocking strategy is adopted and the harmonic restraint ratio is regulated to 15%.

Besides, the higher order harmonics, especially the odd harmonic of the inrushes of UHV transformer are very abundant. The contents of the third and above harmonics with respect to the scenarios in Table I are presented in Table II. Among which, in each cell with respect to any higher order harmonic of the inrush, three numbers comparted by the line separator denote the harmonic rates of phase A, B, C in sequence, respectively. For example, for the inrush resulting from the energization of the transformer without remnant flux and 0 degree inception angle in phase A, the third harmonic contents of phase A, B, C are 31.1, 46.3, and 25.4, respectively.

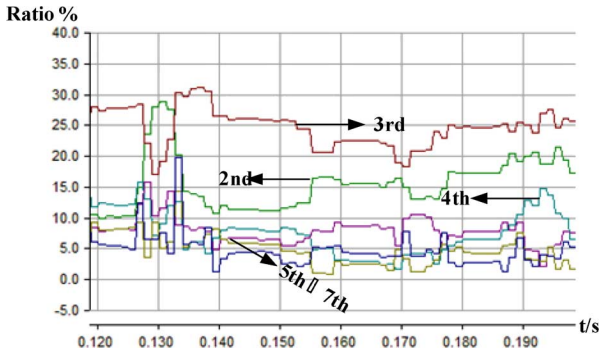

Fig. 10. Harmonic change in the case of energization with remnant flux of A:09 Bm B:0 Bm C:-0.9 Bm with the 30-degree switching angle.

Besides, the change trends of all harmonics with respect to the 8th case in Table I are presented in Fig. 10. The start-time of the waveform is 0.12 s, corresponding to the moment of one cycle after transformer is energized. This is to allow the time window of Fourier algorithm can be filled with all post-fault data to eliminate the edge effect. This is also appropriate to the following figures. As seen, although the second harmonic and other harmonics are relatively low, the third harmonic is quite high and stabilizes above 20%.

It possibly has some impacts on the methods identifying inrush by means of waveform characteristic.

It is impossible to simulate all the conditions involving the diverse initial angles, remnant flux densities and different operation states of systems to validate the existing schemes of the differential protections. However, the simulation results presented in this paper at least suggest that the second-harmonic characteristic of the inrush of UHV transformer is weaker than that in EHV and lower voltage level systems.

This scenario should be paid attention to when the differential protection of the UHV transformer commissions.

C. Simulation and Analysis of Internal Faults

The simulations of interturn short-circuited faults, turn-to-ground fault of various short-circuited turns ratios have been

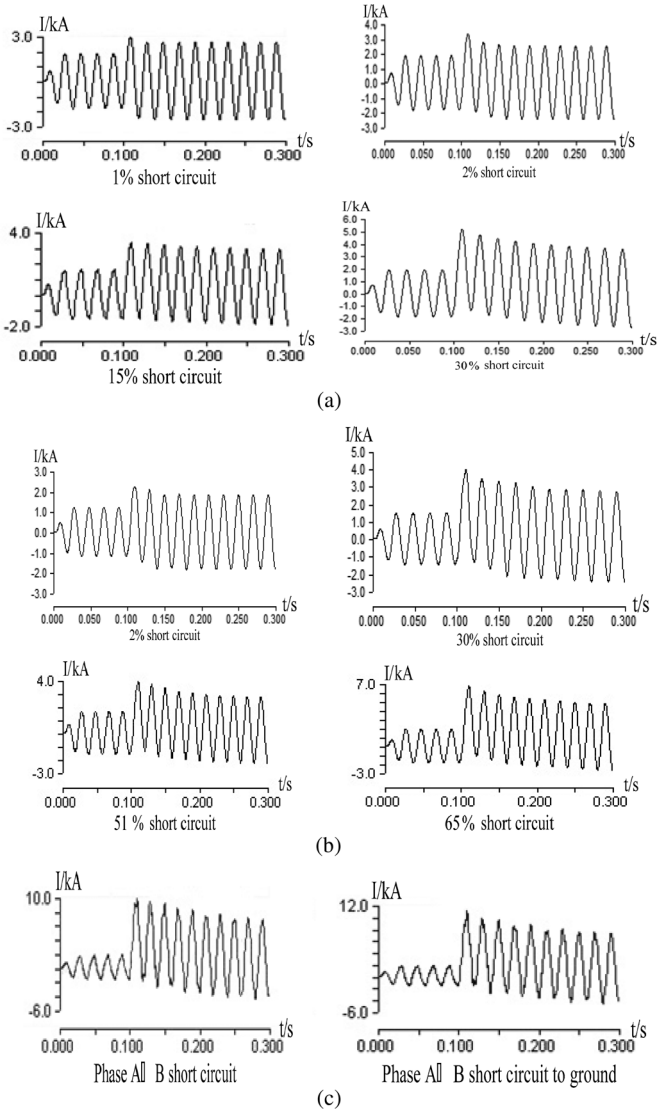

Fig. 11. Phase Currents in the case of internal faults. (a) Interturn short circuit. (b) Short circuit to ground. (c) Lead-out short circuit.

carried out. For simplicity, all the faulty phases are supposed as phase A.

Moreover, several lead-out short-circuited faults are simulated by means of FAULTS module provided by EMTDC, including phase A to ground faults, phase A-B short-circuited faults and phase A-B to ground faults.

Several phase current waveforms of phase A in different fault conditions are shown in Fig. 11.

As seen, no mater for interturn short-circuited faults or for phase to ground faults, the more turns are short-circuited, the higher the primary current is. When the lead-out fault occurs, the fault current is high and distorted.

Accordingly, in order to investigate the operation of the differential protection, the three-side influx currents of transformer should be phase compensated to form the differential current. The second harmonics and higher order of differential currents in manifold fault conditions were analyzed, and some results are given in Tables III and IV. Due to the phase compensation, phase B has no differential current when fault occurred in phase A. As seen in these figures, due to the effect of the distributed capacitance of the UHV transmission line and the particularity of the UHV transformer, abundant harmonics exist within the fault currents. However, except for a case of interturn fault and some turn-to-ground faults, the ratio of the second harmonic of the differential currents of in the case of diversified faults, including interturn faults, are under 15% even though only one cycle time elapses after fault inception. In this case, the common restraint ratio of second harmonic, 15% $\sim$ 20%, is promising to keep unchanged or only be lowered slightly. However, we had better investigate the change trends of the second harmonic in those cases with original second-harmonic ratio exceeding 15% before taking that action.

TABLE III
SECOND-HARMONIC ANALYSIS OF INTERNAL WINDING SHORT-CIRCUITED FAULTS

Fault type	Fault turns ratio	2nd harmonic ratio (%)	
		Phase A	Phase C
Interturn short-Circuited	1%	22.6	22.9
	2%	11.0	10.7
	2.5%	8.0	8.0
	5%	3.7	3.3
	10%	3.2	3.0
	15%	2.7	2.2
	30%	2.4	1.9
Turn--to-ground	2%	22.5	22.8
	5%	21.4	21.2
	10%	20.6	20.3
	30%	19.0	19.7
	51%	4.6	4.6
	52.5%	3.8	3.6
	55%	3.6	3.3
	65%	3.1	2.9

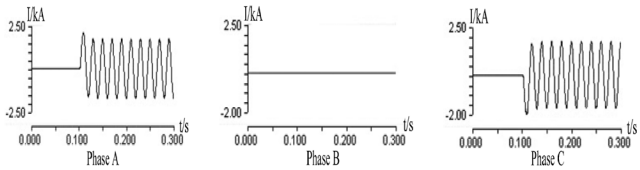

Fig. 12. Differential current in the case of 1% interturn fault.

Therefore, we firstly investigate the case 1% interturn fault. As indicated in Table III, the second harmonic of the differential current of the faulty phase comes to 22.6%, which exceeds the conventional setting value of second-harmonic restraint ratio. The differential current waveform in this scenario is shown in Fig. 12.

Furthermore, the change of the second-harmonic content in this condition is investigated, referring to Fig. 13.

As seen, the second harmonic of the differential current declines rapidly. The second-harmonic ratio is 22.6% after the first post-fault cycle elapses. After that, it decreases to 19% at 21 ms, to 15.3% at 22 ms, to 12.4% at 23 ms, to 10% at 25 ms, and to 7.4% at 26 ms. The time delay is only 6 ms, even if the threshold of restraint ratio is set to be 10%.

TABLE IV
CONTENTS OF HARMONICS OF THIRD AND ABOVE WITH RESPECT TO THE SCENARIO IN TABLE I

Fault type	Fault turns ratio	3rd harmonic ratio (%)	4th harmonic ratio (%)	5th harmonic ratio (%)	6th harmonic ratio (%)	7th harmonic ratio (%)
Interturn short-Circuited	1%	17.4	12.1	8.3	7.3	10.6
	2%	9.1	5.7	3.4	2.2	3.7
	5%	2.4	2.7	2.3	2.1	2.2
	10%	0.4	2.1	2.2	2.2	2.5
	30%	0.4	2.1	2.2	2.1	2.4
Turn--to-ground	2%	17.2	11.9	8.5	5.9	9.0
	5%	18.2	11.9	7.9	5.6	9.1
	10%	18.5	12.9	8.4	5.9	9.6
	30%	21.8	13.0	8.3	4.8	8.5

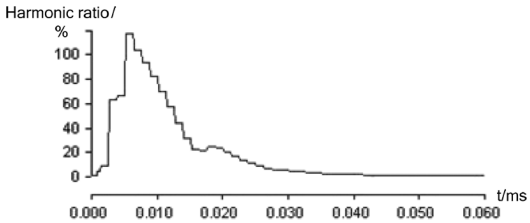

Fig. 13. Second-harmonic curve in the case of 1% interturn fault.

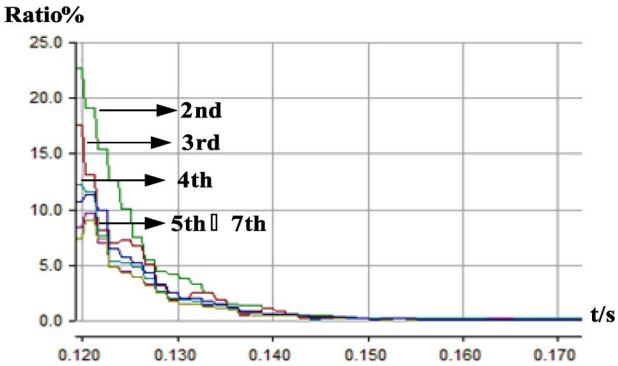

Fig. 14. Harmonic curve in the case of 1% interturn fault.

The detailed higher harmonic change trends in this scenario are illustrated in Fig. 14. As seen, the second harmonic accounts for the maximum portion among all harmonics after one-cycle of fault inception. After that, all harmonics declines and they converge to a same lower limit.

Furthermore, we investigate the harmonic change trends of turn-ground faults, of which original second harmonic exceeds 15%. We take 2% turn-to-ground as an example. As seen in Table III, its original second-harmonic ratios are 22.5% and 22.8%, respectively, for phase A and C at the moment of one-cycle of postfault. Besides, the higher order harmonic contents are quite abundant in this case, as shown in Table IV. However, they decline rapidly. As seen in Fig. 15, the second harmonic within the differential current is high up to 23.3% after one-cycle of fault inception. However, it declines rapidly. It decreases to 17% at 21 ms, to 15.1% at 22 ms, to 10.8% at 23 ms. The changes of other higher order harmonics are similar.

Combined with the analysis of inrush currents, the maloperation probability may be evidently reduced if the second-harmonic restraint ratio declines properly, for example, declining

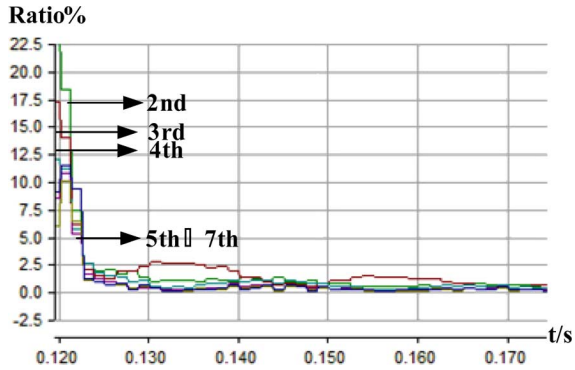

Fig. 15. Harmonic curve in the case of 2% turn-to-ground fault.

to 10%. Meanwhile, it will not influence the operating speed of the differential protection in a mass of fault conditions.

D. Impacts of Long Transmission Line on the Second-Harmonic Content of the Inrush

To investigate the impact of the long transmission line to the second-harmonic content of the differential current, the energizations and the internal faults are re-simulated by comparison between the cases with line or without line. Firstly, the scenarios of energization are studied. Based on Fig. 7, a certain energization is simulated. Then, the distributed capacitance of the transmission line in Fig. 7 is ignored and the total impedance is incorporated into the system impedance. Then, the process of energization is repeated. The comparison between above two cases is illustrated in Fig. 16. As seen, the second-harmonic content and the changing trend are very similar, of which the deviation is within 2%. Furthermore, the transformer is energized from the 500 kV, of which one is with the long line on the 1000 kV and the other is without. The comparison of the second-harmonic contents of these two cases is illustrated in Fig. 17. As seen, these two cases show the similar second-harmonic content the long line is not a key factor to influence the second-harmonic content of inrushes, at least in this system arrangement.

IV. CONCLUSION

Based on the benchmark model of transformer provided by EMTDC, the energization and internal fault models of UHV

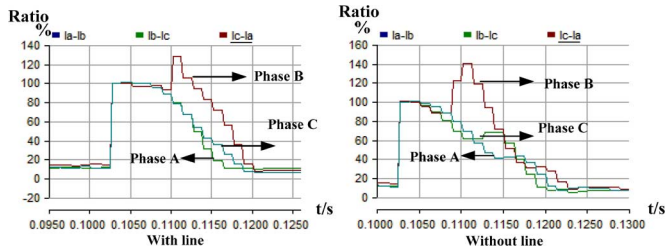

Fig. 16. Comparison of the second-harmonic characteristic in the case of energizations With line and without long line from 1000-kV side.

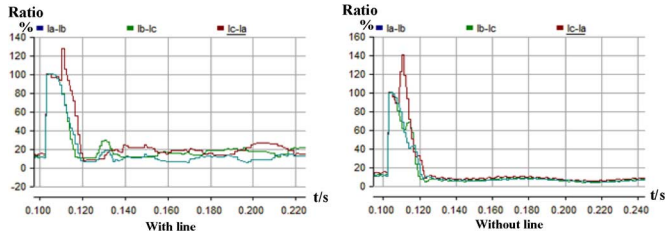

Fig. 17. Comparison of the second-harmonic characteristic in the case of energizations With line and Without long line from 500-kV side.

transformer are established in this paper in terms of autotransformer mode. The corresponding electromagnetic transient simulations in UHV environment are carried out, and reasonable preconditions for investigating the operating performance of the UHV transformer protection are offered. These models are especially suitable for evaluating the applicability of the existing main protections of transformers to the UHV test and demonstration project in China. The emphasis of this paper rests with evaluating the operation reliability of the differential protection based on second-harmonic blocking. It is proven with the simulation results that the harmonic characteristic of the inrush of UHV transformer is weaker than that of the transformer in the system of EHV and lower voltage grades.

A great deal of beneficial works for identifying the inrush from fault current have been reported [11]–[20]. We can assess their adaptability to UHV transformer base on the models of energization and internal fault of UHV transformer proposed in this paper and chose a satisfactory one. Accordingly, the operational level of the differential protection of UHV transformer can be improved further.

According to the simulation results, the second-harmonic based blocking scheme can distinguish between inrush and fault current on the whole. The protection can be reliably blocked during the energization of UHV transformer if the second-harmonic restraint ratio is set below 10%. However, it may lead to some time delay for the response of the differential protection to some scenarios of internal faults. In this sense, the discrimination between the inrush and the fault current of UHV transformer is still a valuable work. Furthermore, we investigate the harmonic change trends. As seen, the higher order harmonic content and the change trends are similar to the second harmonic.

REFERENCES

[1] A. Guzman, Z. Zocholl, G. Benmouyal, and H. J. Altuve, "A current-based solution for transformer differential protection I. Problem statement," *IEEE Trans. Power Del.*, vol. 16, no. 4, pp. 485–491, Oct. 2001.

[2] S. A. Saleh and M. A. Rahman, "Modeling and protection of a three-phase power transformer using wavelet packet transform," *IEEE Trans. Power Del.*, vol. 20, no. 2, pp. 1273–1282, Apr. 2005.

[3] B. Kasztenny and E. Rosolowski, "Modeling and protection of hexagonal phase-shifting transformers—Part II: Protection," *IEEE Trans. Power Del.*, vol. 23, no. 3, pp. 1351–1358, Jul. 2008.

[4] D. Muthumuni, P. G. McLaren, W. Chandrasena, A. Parker, and M. Yu, "Simulation of delta connected current transformers in a differential protection scheme," in *Proc. 7th Int. Conf. Developments in Power System Protection*, 2005, pp. 222–225.

[5] M. Kezunovic and Y. Guo, "Modeling and simulation of the power transformer faults and related protective relay behavior," *IEEE Trans. Power Del.*, vol. 15, no. 1, pp. 44–50, Jan. 2000.

[6] Z. Zhao and Z. Feng, "Digital real time simulation model and digital integral of autotransformer," (in Chinese) *J. TongJi Univ.*, vol. 29, no. 4, pp. 416–420, 2001.

[7] L. Zhao and C. Chen, "Study of model of three phase autotransformer in electric system transient simulation," in *Proc. EPSA* (in Chinese), 2004, vol. 16, no. 1, p. 83.

[8] S. Sun and M. Fang *et al.*, "Development and design of 1000 kV autotransformer," (in Chinese) *Elect. Equip.*, vol. 8, no. 4, pp. 6–10, 2007.

[9] T. Yang, C. Shi, and X. Tan, *Autotransformer and Its Applications* (in Chinese). Beijing, China: China Electric Power Press, pp. 28–30.

[10] W. Wang and B. Hou, *Theoretical Basis of the Protection Principle of the Utility-Type Unit* (in Chinese). Beijing, China: China Electric Power Press, pp. 63–64.

[11] M. A. Rahman and B. Jeyasurya, "A state-of-the-art review of transformer protection algorithms," *IEEE Trans. Power Del.*, vol. 3, no. 2, pp. 534–544, Apr. 1988.

[12] B. Kasztenny, "Impact of transformer inrush currents on sensitive protection functions," in *Proc. IEEE Power Eng. Soc. Transmission and Distribution Conf. and Exhib. 2005/2006*, 2006, pp. 820–823.

[13] A. Guzman, S. Zocholl, G. Benmouyal, and H. J. Altuve, "A current-based solution for transformer differential protection. II. Relay description and evaluation," *IEEE Trans. Power Del.*, vol. 17, no. 4, pp. 886–893, Oct. 2002.

[14] B. Kasztenny and M. Kezunovic, "Digital relays improve protection of large transformers," *IEEE Comput. Applic. Power*, vol. 11, no. 4, pp. 39–45, 1998.

[15] M. A. Rahman and P. K. Dash, "Fast algorithm for digital protection of power transformers," *IEE Proc. C: Gener., Transm., Distrib.*, vol. 129, no. 2, pp. 79–85, 1982.

[16] T. Hayder, U. Schaerli, K. Feser, and L. Schiel, "Universal adaptive differential protection for regulating transformers," *IEEE Trans. Power Del.*, vol. 23, no. 2, pp. 568–575, Apr. 2008.

[17] Y. C. Kang, B. E. Lee, S. H. Kang, and P. A. Crossley, "Transformer protection based on the increment of flux linkages," *IEE Proc. C: Gener., Transm., Distrib.*, vol. 151, no. 4, pp. 548–554, 2004.

[18] J. Faiz and S. Lotfi-Fard, "A novel wavelet-based algorithm for discrimination of internal faults from magnetizing inrush currents in power transformers," *IEEE Trans. Power Del.*, vol. 21, no. 4, pp. 1989–1996, Oct. 2006.

[19] L. Kojovic, M. T. Bishop, and D. Sharma, "Innovative differential protection of power transformers using low energy current sensors," in *Proc. IEEE Ind. Appl. Soc. Annu. Meeting*, 2009, pp. 1–8.

[20] W. Chandrasena, P. G. McLaren, R. P. Jayasinghe, D. Muthumuni, E. Dirks, and A. Parker, "Simulation of differential current protection schemes involving multiple current transformers and a varistor," in *Proc. IEEE Power Eng. Soc. Summer Meeting*, 2001, vol. 2, pp. 1169–1174.

Xiangning Lin (SM'08) received the Master's and Ph.D. degrees from Huazhong University of Science and Technology (HUST), Wuhan, China, in electrical engineering.

He is currently a Professor at HUST and "Chutian Scholar" with Three Gorges University, Yichang, Hubei Province, China. His research interests are modern signal processing and its applications in the power systems, power system protective relaying, and control.

Jingguang Huang is currently pursuing the Ph.D. degree at Huazhong University of Science and Technology (HUST), Wuhan, China.

He is an Associate Professor in the Department of Electrical Engineering, College of Electrical Engineering and Information Technology, China Three Gorges University (CTGU), Yichang, Hubei Province, China. His research interests include power systems, power system protective relaying, and control.

Linjun Zeng received the Bachelor's and Master's degrees from China Three Gorges University (CTGU) in 2006 and 2009, respectively.

His research interests are power system protection and control.

Zhiqian Q. Bo (SM'95) received the B.Sc. degree from Northeastern University, Shenyang, China, in 1982 and the Ph.D. degree from The Queen's University of Belfast, Belfast, U.K., in 1988.

From 1989 to 1997, he was with the Power Systems Group, University of Bath, Bath, U.K. Currently, he is with AREVA T&D—Automation and Information Systems, Stafford, U.K., responsible for new technology developments. His main research interests are power system protection and control.